HAL
open science

Joint evolution of equatorial oscillation and interhemispheric circulation in Saturn's stratosphere

Deborah Bardet, Aymeric Spiga, Sandrine Guerlet

To cite this version:

Deborah Bardet, Aymeric Spiga, Sandrine Guerlet. Joint evolution of equatorial oscillation and interhemispheric circulation in Saturn's stratosphere. Nature Astronomy, 2022, 10.1038/s41550-022-01670-7 . hal-03690475

HAL Id: hal-03690475

https://ens.hal.science/hal-03690475v1

Submitted on 8 Jun 2022

HAL is a multi-disciplinary open access archive for the deposit and dissemination of scientific research documents, whether they are published or not. The documents may come from teaching and research institutions in France or abroad, or from public or private research centers.

L'archive ouverte pluridisciplinaire **HAL**, est destinée au dépôt et à la diffusion de documents scientifiques de niveau recherche, publiés ou non, émanant des établissements d'enseignement et de recherche français ou étrangers, des laboratoires publics ou privés.

Joint evolution of equatorial oscillation and inter-hemispheric circulation in Saturn's stratosphere

Deborah Bardet[1,*], **Aymeric Spiga**[1,2], **and Sandrine Guerlet**[1,3]

[1]Laboratoire de Météorologie Dynamique / Institut Pierre-Simon Laplace (LMD/IPSL), Sorbonne Université, Centre National de la Recherche Scientifique (CNRS), École Polytechnique, Institut Polytechnique de Paris, École Normale Supérieure (ENS), PSL Research University, Paris, France
[2]Institut Universitaire de France (IUF), Paris, France
[3]LESIA, Observatoire de Paris, Université PSL, Centre National de la Recherche Scientifique (CNRS), Sorbonne Université, Université de Paris, Meudon, France
[*]deborah.bardet@lmd.ipsl.fr

ABSTRACT

Planetary stratospheres are characterized by a subtle interplay between dynamics, radiation, and chemistry. Observations of Saturn's stratosphere revealed a semi-annual equatorial oscillation of temperature and hinted at an inter-hemispheric circulation of hydrocarbon species. Both the forcing mechanisms of the former and the existence of the latter have remained debated. Here we use a new troposphere-to-stratosphere Saturn global climate model to argue that those two open questions are intimately connected. Our Saturn climate model reproduces a stratospheric oscillation exhibiting the observed semi-annual period, amplitude, and downward propagation. In the same Saturn simulation, a prominent stratospheric summer-to-winter hemispheric circulation develops at solstices, controlled by both the seasonal radiative gradients and Rossby-wave pumping in the winter subsiding branch, analogous to Earth's Brewer-Dobson circulation. Furthermore, we show that Saturn's equatorial oscillation is driven by the seasonal variability of both the resolved planetary-scale wave activity and the inter-hemispheric circulation, akin to Earth's Semi-Annual Oscillation.

An important recent finding in Saturn's atmospheric science is the discovery of an equatorial oscillation in its stratosphere[1–3]. Temperature retrievals by infrared spectroscopy revealed a semi-annual oscillation consisting in a downward propagation of local extrema of equatorial stratospheric temperatures and inferred winds over seasonal timescales[3–8].

Saturn's semi-annual equatorial oscillation (≈15 Earth years for its ≈30 Earth year orbital period) is reminiscent of the Earth's stratospheric Quasi-Biennial Oscillation (QBO) and Semi-Annual Oscillation (SAO)[9–11] and Jupiter's equatorial quasi-quadrennial oscillation (QQO)[12–15]. While the Earth's QBO extends from the lower stratosphere down to the tropopause, the Earth's SAO occurs from the mesosphere down to the high stratosphere. Equatorial oscillations result from interactions between the mean zonal flow and planetary waves – such as Rossby, Kelvin, inertia-gravity, Rossby-gravity waves – and mesoscale gravity waves[9–11,16–18]. Furthermore, the Earth's SAO undergoes a seasonal forcing originating from the Brewer-Dobson circulation, a summer-to-winter hemispheric circulation, that forces the westward phase during solstitial cross-equatorial transport and the eastward phase during equinoctial overturns.

The nature of Saturn's equatorial oscillation remains uncertain, hence the variety of names given in the literature: QBO-like[19], SAO-like[2], or quasi-periodic[20]. This is mainly due to its similarities with both the Earth's QBO and SAO[3,9–11]. On the one hand, the downward propagation of Saturn's equatorial oscillation extends, akin to Earth's QBO, almost down to the tropopause[5]. On the other hand, its semi-annual periodicity advocates for a seasonal forcing and hints at an SAO-like mechanism[3]. The conditions for upward propagation of planetary-scale waves, together with their seasonal variations, has been partly characterized[3,21,22], but the wave-mean flow interactions remain to be quantified to address the open question of the nature of Saturn's equatorial oscillation.

The existence of an analog of the Earth's Brewer-Dobson circulation in Saturn's stratosphere has remained elusive. Observations of anomalies in temperature and hydrocarbons concentration at the winter tropics[23–27] were interpreted as the downwelling branch of a seasonally-dependent meridional stratospheric circulation[23,28], reminiscent of the Earth's Brewer-Dobson circulation. However, both the overall structure of this putative meridional circulation in Saturn's stratosphere, and its

possible role in the forcing of the oscillation, remain completely unknown.

To characterize the nature and leading mechanisms of Saturn's stratospheric dynamics, modeling is of key importance. Three-dimensional modeling using artificial eddy forcing[29] featured a seasonal equator-to-subtropics cell qualitatively consistent with the measured anomalies in the winter tropics, but without reproducing any kind of periodic equatorial oscillation. Idealized three-dimensional Global Climate Model (GCM) for brown dwarfs and gas giants using a simple random forcing to generate waves[19] demonstrated the emergence of a stratospheric equatorial oscillation driven by planetary and meso-scale waves. A previous version of our three-dimensional Saturn GCM[30] showed an equatorial oscillation forced by resolved planetary-scale waves, maintained by seasonal cycle and influenced by ring shadowing. Nevertheless, the coarse vertical resolution in this GCM produced an irregular periodicity which prevented demonstrating the nature of Saturn's equatorial oscillation and exploring the possibility of stratospheric inter-hemispheric circulation.

Here we propose to address these open questions with new simulations with the DYNAMICO-Saturn GCM[30,31] (see Methods). Our methodology is a combination of fine scale dynamics permitting a spontaneous emergence of eddies and planetary-scale waves, tailored seasonal radiative transfer for Saturn, and adequate stratospheric vertical resolution (96 instead of 61 levels for the same pressure domain than ref.[30], 3 bar to 1 μbar). We provide, in a single simulation, a consistent picture of key dynamics in Saturn's stratosphere: we report on the nature of the stratospheric oscillation that develops without prescribed wave forcing; we describe the seasonal inter-hemispheric circulation obtained in our model; and we eventually highlight interactions in between.

Saturn's stratospheric equatorial oscillation

An equatorial oscillation close to the observed Saturn equatorial oscillation is reproduced by our model. The modeled equatorial zonal wind displays a stack of alternating eastward and westward wind direction over the vertical (Figure 1a). This wind structure moves downward with time with a semi-annual periodicity, from 0.5 to 10^3 Pa, with a "staircase" behavior (Figure 1b): between two descent episodes, the zonal wind undergoes a plateau phase, locked at a given pressure level for almost a quarter of year, as in the 11th and 12th simulated Saturn years. Eastward and westward wind maxima (hereafter named phases) exhibit a shear of 140 m s^{-1} over a decade of pressure (Figure 1c), which is slightly less than an implied vertical zonal wind shear of the order of 150 to 250 m s^{-1} derived, using the thermal-wind equation, from the observed temperatures between the equator and 15° of latitude[3]. Overall, the oscillation of eastward and westward phases is recurring over the last four simulated Saturn years. The periodicity of this wind oscillation depends on the pressure level: 0.5-year period at altitudes of 5 and 10 Pa and closer to 1-year at altitudes ranging between 20 to 100 Pa. A stack of alternating local temperature extrema at the equator and $\pm 20°$ of planetocentric latitude (Figures A.1 and A.2), which propagate downward over time (Figure A.3) is also reproduced by our model. These strong meridional temperature gradients, changing sign with altitude, are consistent with the strong vertical shear of zonal wind at the equator (Figures 1b and 1c), and are reminiscent of Cassini observations[3]. The temperature oscillation has the same periodicity as the zonal wind oscillation. This periodic evolution is comparable to the one observed from ground-based telescopes[2] (Figure A.4).

Both the vertical structure and the downward propagation of the equatorial oscillation phases are controlled by the forcing of waves resolved by the model. To highlight this effect, we compute the acceleration of the zonal wind driven by wave saturation or breaking (given by the Eliassen-Palm Flux divergence that represent eddy forcing, hereafter named EPF) and by the residual mean circulation (hereafter named RMC), the two main dynamical forcing sources, using the Transformed Eulerian Mean (TEM) formalism (see Eq 3 and Methods for detail). As an example, the descent from 2 to 5 Pa of the westward jet during the 9th simulated Saturn year (Figure 1c) is due to an eastward forcing from EPF and RMC in this pressure interval (Figure 1d). These cumulative eastward forcings during 1000 Saturn days before year 9.5 drive the zonal-mean zonal wind in eastward direction and produce the eastward phase change at 9.5-year between 2 and 5 Pa. Moreover from 5 to 11 Pa, RMC induces a westward forcing on the zonal wind that produces a westward phase peaking at -90 m s^{-1}. Around 2 Pa, the above eastward forcing slows down the westward jet, while the westward forcing just below the 2-to-5-Pa westward jet accelerates the flow around 10 Pa, resulting in the downward propagation of the westward phase.

Planetary-scale waves resolved by our DYNAMICO-Saturn model drive the equatorial oscillation phases and its downward propagation, as is partly the case for the Earth's QBO and SAO. We demonstrate this with two-dimensional Fourier transforms of zonal and meridional winds[32] in which we identify the waves involved in driving the equatorial oscillation (see Methods for details). Planetary-scale Rossby waves (lowest frequency and westward in Figure 1f) are the main source of westward wave forcing; other key wave forcing is provided by Rossby-gravity waves (highest frequency and westward in Figure 1g) and inertia-gravity waves (highest frequency in Figure 1f). Inertia-gravity waves are a westward and eastward forcing source for the mean flow. The main eastward wave forcing comes from the Kelvin waves (lowest frequency and eastward in Figure 1f).

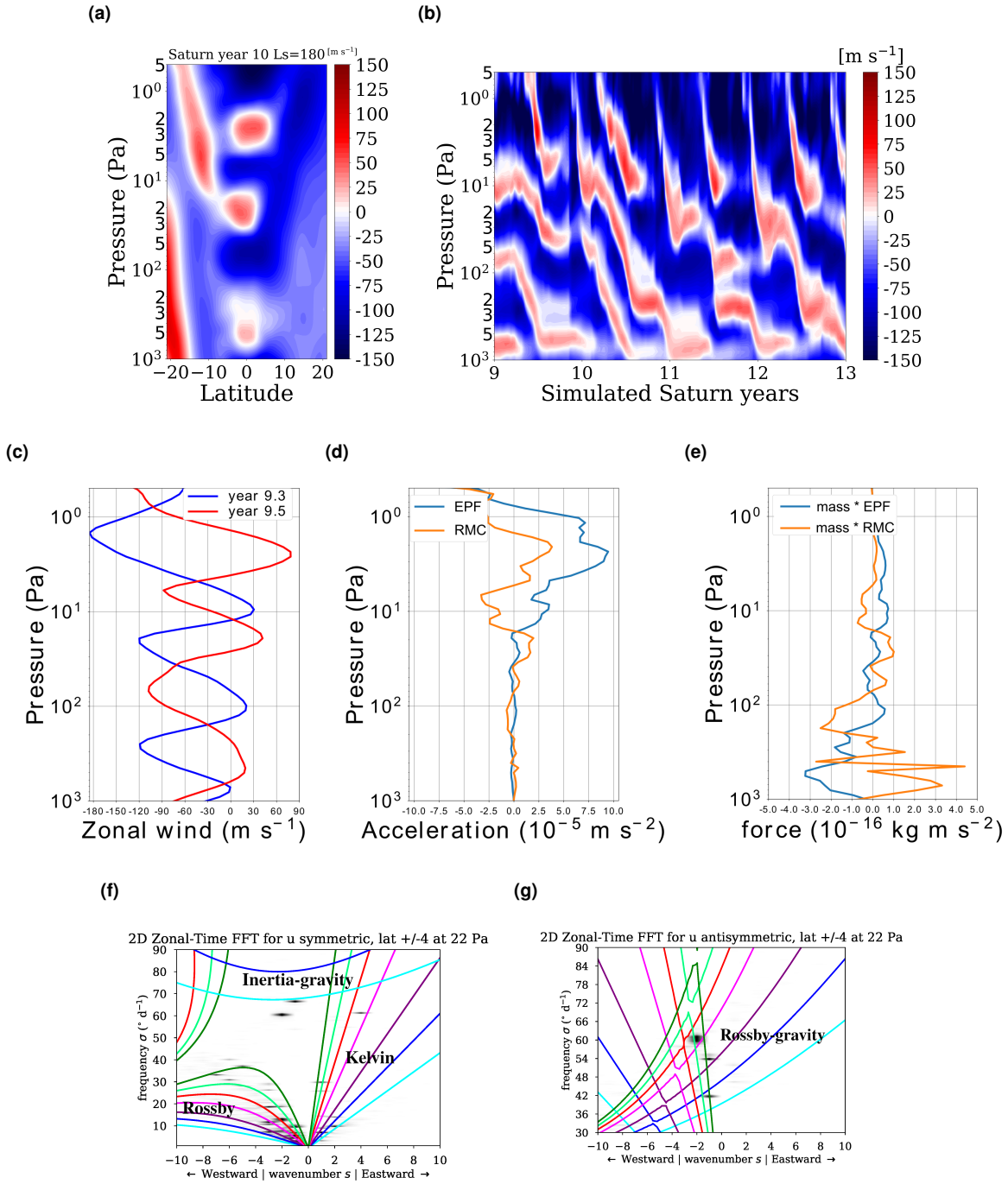

Figure 1. Eddy-to-mean flow interactions at the origin of the time evolution of Saturn's equatorial oscillation. 1a, Altitude-latitude cross-section of the zonal-mean zonal wind at Ls=180° of the tenth simulated Saturn year. 1b, Altitude-time cross-section of the zonal-mean zonal wind at the equator for the last four simulated Saturn years. 1c, Zonal-mean zonal wind profiles at 9.3 simulated Saturn year (blue line) and at 9.5 simulated Saturn year (red line). These profiles are averaged between ±2° of latitude. 1d, One-thousand-day temporal mean of the zonal-mean eddy-induced acceleration (blue line, term EPF of Eq. 3) and of the zonal-mean RMC-induced acceleration (orange line, term RMC of Eq. 3) profiles to highlight dynamical forcing responsible of the 9.5-year zonal-mean zonal wind profile.These profiles are averaged between ±3° of latitude. 1e, same as 1d but multiply by the atmospheric layers' mass. 1f-1g Two-dimensional Fourier transform at 22 Pa of the symmetric and antisymmetric component of the zonal wind to highlight equatorial planetary-scale waves[32] involved in the equatorial oscillation forcing. Gray shaded areas depicts the waves identified by the spectral analysis. Color curves represent dispersion relation from the linear theory. Seven equivalent depths are used for theoretical curves: 5 km (cyan), 10 km (blue), 20 km (purple), 50 km (magenta), 100 km (red), 200 km (light green), 500 km (dark green).

Saturn's stratospheric inter-hemispheric circulation

Our model simulations for Saturn exhibit clear-cut inter-hemispheric transport in the stratosphere. At northern winter solstice (Figure 2a), DYNAMICO-Saturn develops a circulation from the southern hemisphere to the northern hemisphere; this circulation is reversed at northern summer solstice (Figure 2e). Although they have the same vertical extent (from 10^3 to 10^1Pa), the solstice circulations differ by their intensity: the northern winter amplitude peaks at about 45 Pa m s^{-1} while the southern winter amplitude only at 20 Pa m s^{-1}. This asymmetry in the circulation intensity may result from the orbital eccentricity, which produces a southern summer warmer than the northern summer, inducing a more significant south-to-north circulation. At solstices, the main descending branch of the inter-hemispheric circulation modeled by DYNAMICO-Saturn (Figure 2a and Figure 2e) is located in the same latitude region (15 to 25°) as the warm temperature anomaly and the high concentration of hydrocarbons observed by Cassini[23–27] that is, at low winter latitudes. Regarding the higher latitudes, several small-scale cells, with a circulation intensity under 5 Pa m s^{-1}, are associated to high-latitude jets extending to 10^2 Pa.

The downwelling branch of the inter-hemispheric circulation at mid-winter latitudes results from planetary-scale Rossby waves producing a westward wave forcing in the winter hemisphere. During the northern winter (Figure 2b), a peak of negative eddy-induced acceleration (EPF term in equation 3), culminating at -0.8$\times 10^{-5}$ m s^{-2} at 10 Pa, occurs at the same latitudes as the descending branch of the inter-hemispheric circulation. Similar behavior happens during the northern summer (Figure 2f), where the descending branch is correlated to a powerful westward wave forcing, about -1$\times 10^{-5}$ m s^{-2}. The downwelling branches of the meridional circulation appear to originate from westward wave forcing. This interpretation is reinforced by the seasonality of the Rossby waves (Figure A.5). During northern winter, the Rossby wave activity is much higher in the northern tropics (Figure A.5b) than in the southern hemisphere (Figure A.5a). This asymmetry is reversed at the northern summer, where the Rossby wave activity is enhanced in the southern (winter) tropics (Figure A.5e) and reduced in the summer tropics (Figure A.5f). Together with the westward wave forcing occurring for the descending branch, the presence of Rossby waves at these latitudes shows the Rossby waves breaking and hints for the "Rossby-wave pump"[33–36] involved in the poleward flow forcing of the Brewer-Dobson circulation on Earth. In short, the "Rossby-wave pump" is a westward drag at mid- to high winter latitudes induced by the dominant Rossby waves, causing the descent at middle winter latitudes (to conserve angular momentum).

The overturning of the inter-hemispheric circulation occurs twice a year, at the equinoxes. At northern spring equinox (Figure 2c), the DYNAMICO-Saturn model depicts two symmetric cells composed by a single, common, upwelling branch centered at the equator and two downwelling branches located around 40°N and 40°S. The two symmetric cells represent a mass flux which does not exceed 10 Pa m s^{-1} per unit of density. The single equatorial upwelling is associated to a pronounced shear of westward and eastward eddy-induced acceleration (EPF term in equation 3, in Figure 2d), between $\pm 1.5\times 10^{-5}$ m s^{-2}, from 10^2 and 10^1 Pa. The stack of westward and eastward acceleration is characteristic of a vertical stack of eastward- and westward-forcing waves at the equator. This configuration is reminiscent of the stratospheric circulation on Earth's northern spring, with a single equatorial ascending branch[33,35,36]. The northern autumn overturning is disturbed by the persistence of the cross-equatorial circulation established during the northern summer, which induces a temporal shift in the development of this reversal. A circulation equivalent to the northern summer solstice persists, if we consider a seasonal average centered at Ls=210°. However, if we consider the average between Ls=190° and Ls=280° (Figure 2g), a similar configuration to the northern spring equinox (Figure 2c) is evidenced with a slight enhancement in equator-to-south circulation intensity (peaked at -30 Pa m s^{-1}), but focused on a narrower pressure range (between 10^3 to 10^2 Pa), and a single ascending branch moved to 10°N. This suggests that there is a temporal lag of 30 to 60° of Ls in the autumnal reversal. Analysis of wave forcing during the northern autumn equinox (Figure 2h) depicts a significant negative drag from southern tropical to southern high latitudes, which is similar to the summer solstice configuration (Figure 2f), with a slight decrease in the eastward and westward wave forcing at the equator. The persistence of solstice-like forcing during the northern autumn equinox implies that the expected inter-hemispheric circulation overturning is incomplete during this season (Figure 2g).

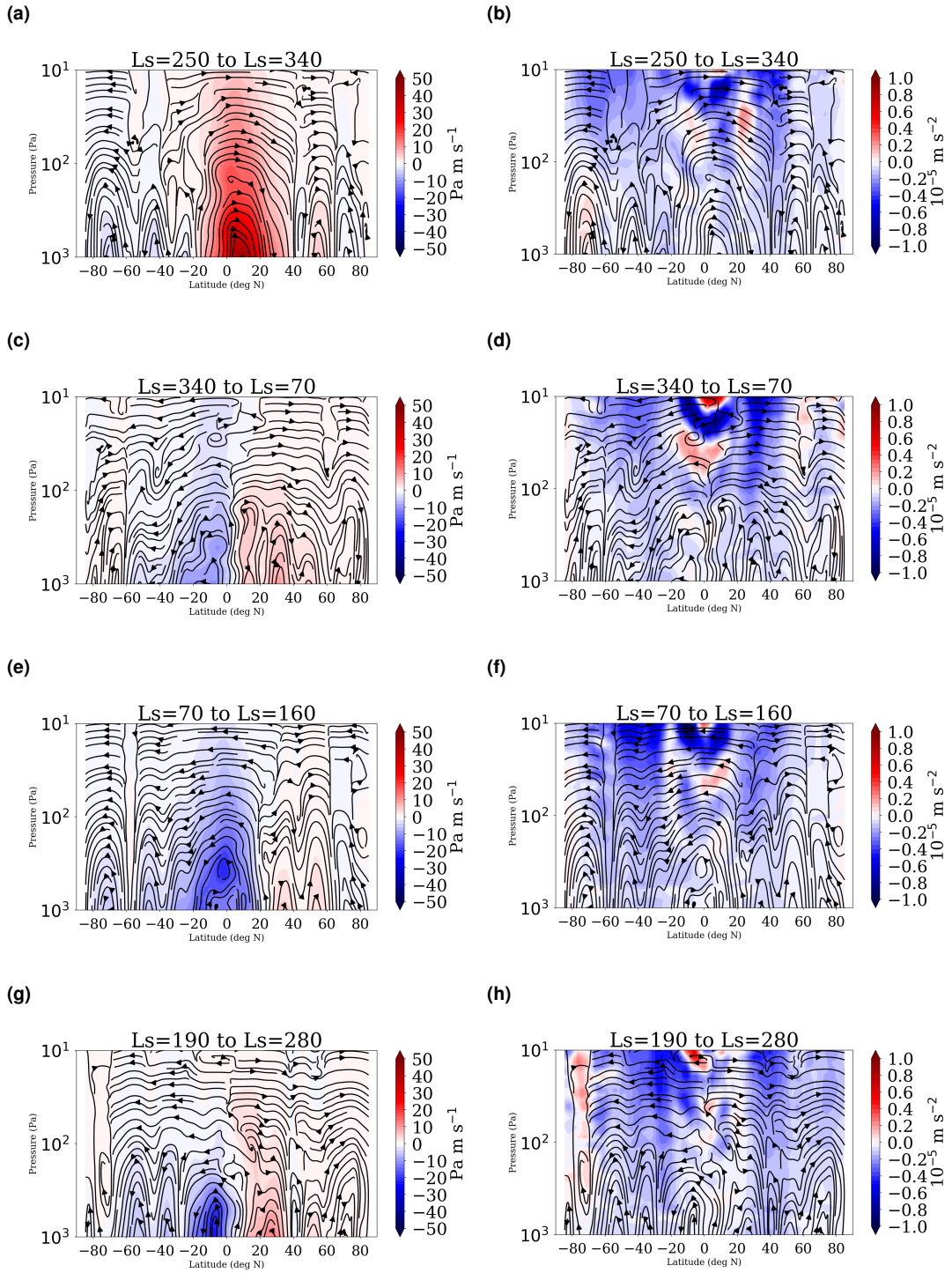

Figure 2. Circulation during different seasons and the main acceleration terms driving it. Seasonal- and zonal-mean Transformed Eulerian Mean stream function (2a, 2c, 2e, 2g) and eddy-induced acceleration (2b, 2d, 2f, 2h) for the northern: winter solstice (2a and 2b) from Ls=250° to Ls=340°, spring equinox (2c and 2d) from Ls=340° to Ls=70°, summer solstice (2e and 2f) from Ls=70° to Ls=160° and autumn equinox (2g and 2h) from Ls=190° to Ls=280°. The seasonal mean for the autumn equinox is shifted by 30° of Ls to clearly bring out the fall overturn that occurs later in the season compared to the spring overturn. The TEM stream function is calculated by integrating Eq. 1 (normalized by the density ρ_0) downward from the top level, assuming $\overline{v^*}$ is zero above that level[35]. The sign of the TEM stream function defines the direction of circulation: positive values correspond to a south-to-north circulation and negative values correspond to a north -to-south circulation. Also, the sign of the eddy-induced acceleration defines the direction of the forcing: positive values correspond to an eastward forcing and negative values correspond to a westward forcing. Superimposed streamlines represent the residual mean circulation ($\overline{v^*}$, $\overline{\omega^*}$; Methods). TEM stream functions, eddy-induced acceleration and residual mean circulation are displayed for a typical simulated year, defined by the average of the last nine simulated Saturn years. We also used a 20-grid-point running mean across latitudes to smooth the small-scale dynamics and highlight the residual mean circulation.

The interplay between the equatorial oscillation and the inter-hemispheric circulation

Analyzing further our Saturn simulation results, we highlight an intimate link between the two main stratospheric phenomena discussed thus far: equatorial oscillations and inter-hemispheric circulations. To that end, we combine dynamical forcing analysis (with EPF and RMC) with a seasonal wave activity study depicted by spectral and eddy kinetic analysis at the equator (see Figures A.6, A.7, A.8 and A.9). From this, we design the schematic representation of the seasonal Saturn's stratospheric dynamics in Figure 3.

During solstice seasons (Figure 3a), the westward phase of the equatorial oscillation results from both the westward forcing of the trapped Rossby waves at the equator and the forcing of Rossby waves generated at mid-latitudes (also involved in the "Rossby-wave pump") whose westward deposition of momentum is carried out by the interhemispheric circulation transporting mass and momentum flux from the summer tropics to the equator (Figures A.6 and A.8). As an example, during the northern winter, the westward phase of the equatorial oscillation, around 10 Pa, is correlated to a negative RMC-induced acceleration at summer tropics and a positive RMC-induced acceleration at winter tropics, associated to the summer-to-winter circulation. The equator acts as a frontier, where the entire westward momentum transported from the highest summer latitudes is deposited. Beyond the equator towards the highest winter latitudes, the inter-hemispheric circulation carries only eastward momentum which forces a strong prograde jet correlated to the rings' shadow (already noticed in ref.[30]). The location of the rings' shadow (and associated abrupt change in radiative heating) is correlated with the location of the main downwelling branch of the seasonal circulation in our model, as well as with the associated high Rossby wave activity (Figure A.5). Spectral analysis at the equator demonstrates a wave activity mainly composed of westward-forcing Rossby waves (Figure A.6c). The northern summer solstice exhibits in our simulation the same behavior as the northern winter solstice (see Additional Data Figure A.8).

As is the case on the Earth's stratosphere, the reversals of the modeled inter-hemispheric circulation near the equinoxes are associated to the transition to the eastward phase of Saturn's equatorial oscillation, through the transport and deposition of eastward momentum from Kelvin waves from the troposphere. The combination of the two equinoctial shear zone on either side of the equator in the RMC-induced acceleration (Figures A.7a and A.9a) and the wave forcing EPF shear centered at the equator (Figures 2d and 2h) are characteristic of a phase change of the equatorial oscillation in the upper stratosphere. Furthermore, an eddy kinetic energy maximum is located at the equator (Figure A.7b), which is consistent with the fact that at equinoxes, the equatorial oscillation is driven by planetary waves, with insignificant contribution from the RMC. The development of the eastward phase, just below 10 Pa at northern spring equinox, results from a dissipation of westward-forcing Rossby waves and an enhancement of eastward-forcing Kelvin waves (Figure A.7c), whose propagation is facilitated by the upwelling centered at the equator[37–40]. Kelvin waves drive the equatorial zonal wind because of the absence of the residual mean circulation crossing the equator and depositing westward momentum originating from mid-latitudes. A similar behavior as the northern spring equinox is observed at the northern autumn equinox (see additional Figures A.9b to A.9c).

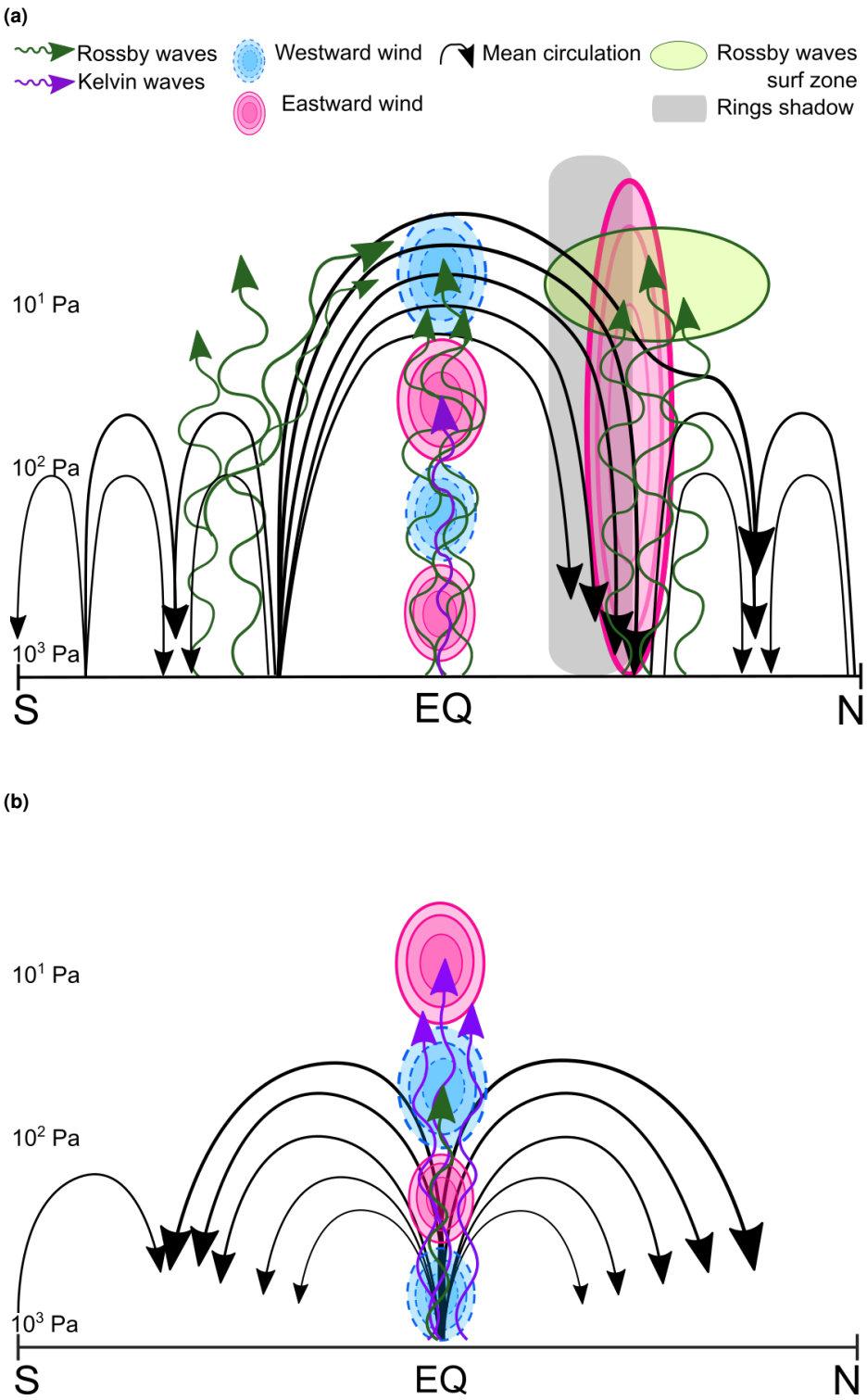

Figure 3. Schematic of the inter-connection between Saturn's equatorial oscillation and its seasonal inter-hemispheric circulation. 3a Saturn's stratospheric dynamics during the northern winter. During the solstices, the forcing of the westward phase of the equatorial oscillation results both from Rossby waves trapped at the equator and from Rossby waves generated at mid-latitudes (also involved in the "Rossby wave pump") whose forcing is carried by the inter-hemispheric circulation. 3b Saturn's stratospheric dynamics during equinoctial seasons (spring and fall). During these seasons, the eastward-phase forcing of the equatorial oscillation occurs during the inter-hemispheric circulation reversal that allow the transport and deposition of the eastward momentum of tropospheric Kelvin waves. Size of arrows shows an approximate propagation of the waves before they reach their breaking altitude.

Conclusion

In our GCM simulations, Saturn's stratospheric equatorial oscillation is reproduced with a periodicity and a vertical extent consistent with observations. This oscillation is mainly driven by planetary-scale waves and the inter-hemispheric circulation. Furthermore, our modeling results exhibit solsticial inter-hemispheric circulations that offer a natural explanation for transport processes suggested from stratospheric Cassini observations. The two phenomena arise naturally from the wave-mean flow dynamics in the stratosphere and their respective seasonality appears closely connected. This leads us to conclude that Saturn's equatorial oscillation bears more resemblance with the Earth's SAO than the Earth's QBO, as it is forced by planetary-scale waves and by the seasonal inter-hemispheric circulation.

Our simulations did not require gravity waves to reproduce an oscillation similar to Saturn's, and its half-year period is well related to seasonal effects. On Jupiter, conversely, the role of gravity waves in forcing the QQO[12,13,41,42] could be dominant[43], similarly to the QBO forcing on Earth. The modeling approach developed here for Saturn would be beneficial to the study of Jupiter's equatorial oscillation, too. Moreover, simulating the stratospheric dynamics of Jupiter and Saturn with the same modeling platform would open perspectives for comparative studies between the two gas giants.

The DYNAMICO-Saturn model is thus able to emulate a plausible stratospheric dynamics leading to the observed signatures. As a follow-up, such a modeling tool could allow us to broaden our understanding of the major dynamical changes caused by exceptional events observed by Cassini and ground-based telescopes, such as the warm stratospheric temperature anomaly[44–46] and the disruption of the equatorial oscillation[20] both resulting from Great White Storms. Our simulations could also provide guidance for future observations of temperature and wind in gas giants' stratosphere[47,48].

Methods

DYNAMICO-Saturn GCM

We employ the DYNAMICO-Saturn[31] Global Climate Model (GCM) developed at Laboratoire de Météorologie Dynamique. A Global Climate Model is composed of a dynamical core coupled with physical packages (also named parameterizations). The dynamical core used in our GCM is DYNAMICO, a dynamical core tailored for massively parallel computational resources[49]. DYNAMICO solves the primitive equations assuming a shallow atmosphere. Horizontal discretization is set over an quasi-uniform icosahedral C-grid. A three-dimensional Hamiltonian approach is employed to formulate DYNAMICO spatial discretization, respecting energy conservation. An explicit Runge-Kutta scheme for the time integration is chosen because of it stability and accuracy. Vertical coordinates are *sigma* levels, mass-based coordinates defined as p/p_b, where p_b is the pressure at the bottom of the model.

Another characteristic of DYNAMICO enhancing the efficiency of numerical computation is the XIOS library (XML Input/Output Server[50,51]). The XIOS library manages all input/output operations independently from the numerical integrations. In particular, directly at model runtime, XIOS converts the dynamic fields computed in the non-conformal icosahedral DYNAMICO grid to a regular latitude-longitude grid, using finite-volume weighting functions.

The DYNAMICO dynamical core is interfaced to physical packages designed for Saturn, particularly its seasonal radiative transfer[52]. Radiative computations are based on a versatile correlated-k method[53–55], with k-coefficient derived from detailed line-by-line computations based on HITRAN spectroscopy database[56]. Methane, ethane and acetylene (the three main hydrocarbons accounting for heating and cooling in the stratosphere) are taken into account in radiative contributions, as well as H_2-H_2 and H_2-He collision-induced absorption[57] and tropospheric and stratospheric aerosols layers. Radiative computations account for ring shadowing as well as internal heat flux independent with latitude[52]. At mid and high latitudes, GCM temperature outputs are very close to the radiative-convective model ref.[52] with a 40-K meridional gradient between summer and winter hemispheres.

To mitigate the sub-grid scale (unresolved) turbulent cascade of energy towards the smaller scales in the horizontal dimension, an additional hyperdiffusion term is added in the vorticity, divergence and temperature equations. Along the vertical dimension, the sub-grid scale energy cascade is processed by a combination of a diffusion scheme[58] for the small-scale turbulence and a dry convective adjustment scheme[59] for the organized turbulence (for instance, convective plumes).

The simulations analyzed in this study are performed using DYNAMICO-Saturn with a horizontal resolution of 1/2° in latitude and longitude. This resolution is justified by the need to resolve small-scale eddy arising and the inverse energetic cascade to obtain jets driven by geostrophic turbulence[31,60]. Vertical coordinate is discretized over 96 vertical *sigma*-level, corresponding to the pressure range of 3×10^5 Pa to 10^{-1} Pa. The bottom boundary condition at 3×10^5 Pa uses Rayleigh drag and the top boundary condition does not use a sponge layer, as is explained and detailed in ref[31]. We performed a 13 Saturn years duration simulation, starting with a 7 Saturn years spin-up[30,31]. Following the standard of previous papers using DYNAMICO-Saturn, winds are initialized to zero and temperature is initialized to a typical one-dimensional profile obtained with the radiative model of[52].

Transformed Eulerian Mean formalism

Zonal mean circulations, such as the equatorial oscillation and the inter-hemispheric circulation, are driven, on the one hand, by eddy forcing and wave saturation/breaking, and on the other hand, by momentum transport by large-scale meridional circulations. To assess the relative contributions from each phenomena, we analyze results from our GCM by using the Transformed Eulerian Mean (TEM) formalism[10]. The TEM formalism is based on the decomposition of a field as the sum of the zonal mean (denoted by overline in the following equations) and the perturbations (i.e. eddy component, denoted by prime symbol) from this zonal mean. By defining the TEM zonal-mean residual circulation (composed of zonal-mean residual meridional $\overline{v^*}$ velocity in m s^{-1} and vertical $\overline{\omega^*}$ velocity in Pa s^{-1}) as follows[33]:

$$\overline{v^*} = \overline{v} - \frac{\partial}{\partial P}\left(\frac{\overline{v'\theta'}}{\overline{\theta}_P}\right) = -\frac{1}{\rho_0 \cos\phi}\frac{\partial \psi}{\partial P} \tag{1}$$

$$\overline{\omega^*} = \overline{\omega} + \frac{1}{a\cos\phi}\frac{\partial}{\partial \phi}\left(\frac{\cos\phi\,\overline{v'\theta'}}{\overline{\theta}_P}\right) = \frac{1}{a\rho_0\cos\phi}\frac{\partial \psi}{\partial \phi} \tag{2}$$

with Saturn's radius a, density ρ_0, potential temperature θ, latitude ϕ, pressure P and stream function ψ, we obtain the momentum equation in the TEM formalism:

$$\frac{\partial \overline{u}}{\partial t} = \overline{X} - \underbrace{\left[\frac{1}{a\cos\phi}\frac{\partial(\overline{u}\cos(\phi))}{\partial\phi} - f\right]\overline{v^*} - \overline{\omega^*}\frac{\partial \overline{u}}{\partial P}}_{RMC} + \underbrace{\frac{1}{a\cos\phi}\vec{\nabla}.\vec{F}}_{EPF} \tag{3}$$

Acceleration $\frac{\partial \overline{u}}{\partial t}$ on the mean zonal flow $\overline{u}$ can result from either the residual mean circulation $\overline{v^*}$, $\overline{\omega^*}$ (hereafter named RMC term), the eddy forcing and wave breaking/saturation[33,35] expressed by the divergence of the Eliassen-Palm flux $\vec{F}$ (hereafter named EPF term), or the non-conservative friction $\overline{X}$. Components of the Eliassen-Palm flux $\vec{F} = (F^\phi, F^P)$ are defined in equation 4 below.

$$\begin{aligned} F^\phi &= \rho_0 a\cos\phi\left(\overline{v'\theta'}\frac{\frac{\partial\overline{u}}{\partial P}}{\frac{\partial\overline{\theta}}{\partial P}} - \overline{u'v'}\right) \\ F^P &= \rho_0 a\cos\phi\left(\frac{\overline{v'\theta'}}{\frac{\partial\overline{\theta}}{\partial P}}\left(f - \frac{1}{a\cos\phi}\frac{\partial(\overline{u}\cos\phi)}{\partial\phi}\right) - \overline{u'\omega'}\right) \end{aligned} \tag{4}$$

In the absence of friction $\overline{X}$ and wave driving EPF, $\overline{v^*} = \overline{\omega^*} = 0$ and the flow is in steady state (i.e. $\frac{\partial \overline{u}}{\partial t} = 0$). In other words, the terrestrial Brewer-Dobson circulation[33,35,36] described by $\overline{v^*}, \overline{\omega^*}$ is non-zero to maintain steady-state conditions under non-zero wave forcing terms ($\overline{X}$ or EPF) in the momentum equation 3. Hence, the Brewer-Dobson circulation is considered as a wave-driven inter-hemispheric circulation.

Spectral analysis of planetary-scale waves

The characterization of planetary-waves is a key diagnostic to evidence the kind of wave forcing stratospheric circulations. In order to do so in Saturn's stratospheric modeling framework, we use the Wheeler and Kiladis method[32], commonly employed to study terrestrial equatorial waves in the stratosphere[61,62]. This method consists of a two-dimensional Fourier transform, from the longitude - time space to the zonal wavenumber s - frequency σ space of the symmetric (X_S) and antisymmetric (X_A) component of a geophysical field about the equator.

$$\begin{aligned} X_S &= \tfrac{1}{2}\left(X_{10^\circ N} + X_{10^\circ S}\right) \\ X_A &= \tfrac{1}{2}\left(X_{10^\circ N} - X_{10^\circ S}\right) \end{aligned} \tag{5}$$

To capture a representative wave sample of the entire equatorial oscillation, we realize several additional 1000-day-long 1/2° DYNAMICO-Saturn runs, spaced out by 5000 Saturn days, over the 3 last simulated Saturn years. These runs have a daily output frequency, which is 20 times greater than an usual Saturn simulation. For each 1000-day-long runs, we perform the Fourier analysis, then we stack all Fourier transforms power in the complex plane for realizing a combined power signal at a specific frequency, for the last three years of simulation (Figures 1f and 1g) or by seasons (Figures A.5, A.6c, A.7c, A.8c and

A.9c), to obtain a Fourier analysis representative of the equatorial oscillation forcing or mid-latitude waves activity. Contrary to previous work[30,31], which performed Fourier analysis over a single 1000-day-long run, we are able by the stacking technique to clearly identify all kind of waves involved in the equatorial oscillation forcing, even the weakest ones. It is necessary in theory to treat all components of wind and temperature fields because each kind of wave has a different signature in each field. In practice, in the spectral (s, σ) space:

- the symmetric component of zonal wind is commonly used to evidence planetary-scale Rossby, inertia-gravity and Kelvin waves,
- the antisymmetric component of zonal wind is commonly used to evidence Rossby-gravity waves,
- the symmetric component of meridional wind is commonly used to evidence inertia-gravity waves,
- the symmetric component of vertical wind is commonly used to evidence inertia-gravity and Kelvin waves (but this field is often noisy).

In our GCM outputs, the 2D FFT of the symmetric and antisymmetric components of u have clearly shown all these different waves in the stratosphere (displayed in Figure 1f-1g). Symmetric and antisymmetric components of the meridional wind show similar spectral analysis and are not shown here. In practical cases of analysis of stratospheric wave dynamics,the temperature and vertical wind fields are seldom used to study stratospheric dynamics because their wave spectral power far too low compared to the wave spectral power deduced from the zonal wind.

To help identify modeled waves, theoretical dispersion relations for a sample of equivalent fluid layer depth (color lines) are superimposed on Fourier transforms. These theoretical lines are based on the *linear waves theory*[63,64], which defines the way used to resolve momentum equations to determine wave types involved in atmospheric motion. For this purpose, we commonly use the Rotating Shallow Water (RSW) model (but assumptions made for the RSW model are also valid for the 3D Primitive Equations) for a thin layer of fluid (of height h) with constant density with a free surface. Consider a spectrum of small perturbations (η) to the state of the rest for a RSW fluid (of constant height H), one can define the free surface height as $h = H + \eta$. For sufficiently small components of the wind u, v and perturbations η, one can neglect non-linear terms of the momentum equations. Following the Fourier method, which consist in an eigenvalue problem for harmonic waves solutions for $u = u_0 e^{i(wt - \vec{k}.\vec{x})}$, $v = v_0 e^{i(wt - \vec{k}.\vec{x})}$ and $\eta = \eta_0 e^{i(wt - \vec{k}.\vec{x})}$, one obtains an algebraic system after substitution into linearized momentum equations. Theoretical dispersion relations for equatorial waves[62] are the following:

$$\begin{aligned} \sqrt{\gamma}(2\nu+1) &= \gamma\sigma^2 - s^2 - s/\sigma \\ \gamma &= \frac{4a^2\Omega^2}{gh} \end{aligned} \tag{6}$$

where ν is the meridional mode number, γ is named the Lamb parameter, and h is an equivalent depth associated with the vertical wavenumber m:

$$m^2 = \frac{N^2}{gh} - \frac{1}{4H^2} \tag{7}$$

Values of ν defines the considered wave, for example, Rossby waves are defined for ν = +1, +2, ..., Rossby-gravity waves for ν = 0 and Kelvin waves for ν = -1, -2,...

These colored lines describe different "equivalent depth" corresponding to the RSW model constant height H, which is imposed to introduce the small perturbation and the harmonic waves solution. These "equivalent depths" indicate the order of magnitude of the vertical wavenumber (linked to vertical wavelength) of waves in our GCM. To choose these theoretical "equivalent depths", we created a sample of values that encircle the vertical discretization of the GCM to only consider resolved waves.

Data availability

Simulation outputs are too heavy to be shared in a public DOI-based repository. Nevertheless, minimal dataset derived from simulation outputs (zonal averaged eddy-to-mean interaction diagnostics) are made available at the DOI-based data center IPSL-ESPRI at the following link:
https://doi.org/10.14768/6494348c-3304-4838-a379-a7ccfefac872.

Code Availability

The Python codes developed to produce the Transformed Eulerian Mean formalism diagnostics are available in the online repository at https://github.com/aymeric-spiga/dynanalysis

Acknowledgements

The authors acknowledge the exceptional computing support from Grand Equipement National de Calcul Intensif (GENCI) and Centre Informatique National de l'Enseignement Supérieur (CINES). All the simulations presented here were carried out on the Occigen cluster hosted at CINES. This work was granted access to the High-Performance Computing (HPC) resources of CINES under the allocations A0080110391. Bardet, Spiga, Guerlet acknowledge funding from Agence National de la Recherche (ANR), project EMERGIANT ANR-17-CE31-0007. The authors acknowledge Thomas Dubos, Yann Meurdesoif and Ehouarn Millour for key contributions in developing the DYNAMICO-Saturn model, François Lott for insightful comments on terrestrial stratospheric dynamics, and Thierry Fouchet for long-standing support of modeling studies of Saturn's stratosphere.

Author Contributions Statement

D.B. performed the simulations, carried out the analysis (including figures), interpreted the results, and led manuscript writing. A.S. and D.B. developed the post-processing calculations. A.S. and S.G. contributed to the discussions and interpretations of results. All authors designed the methodology and contributed to the manuscript.

Competing Interests Statement

The authors declare no competing interests.

References

1. Fouchet, T. *et al.* An equatorial oscillation in Saturn's middle atmosphere. *Nature* **453**, 200–202, DOI: 10.1038/nature06912 (2008).
2. Orton, G. S. *et al.* Semi-annual oscillations in Saturn's low-latitude stratospheric temperatures. *Nature* **453**, 196–199, DOI: 10.1038/nature06897 (2008).
3. Guerlet, S. *et al.* Equatorial Oscillation and Planetary Wave Activity in Saturn's Stratosphere Through the Cassini Epoch. *J. Geophys. Res. (Planets)* **123**, 246–261, DOI: 10.1002/2017JE005419 (2018).
4. Guerlet, S., Fouchet, T., Bézard, B., Flasar, F. M. & Simon-Miller, A. A. Evolution of the equatorial oscillation in Saturn's stratosphere between 2005 and 2010 from Cassini/CIRS limb data analysis. *Geophys. Res. Lett.* **38**, L09201, DOI: 10.1029/2011GL047192 (2011).
5. Schinder, P. J. *et al.* Saturn's equatorial oscillation: Evidence of descending thermal structure from Cassini radio occultations. *Geophys. Res. Lett.* **38**, L08205, DOI: 10.1029/2011GL047191 (2011).
6. Sánchez-Lavega, A. *et al.* An enduring rapidly moving storm as a guide to Saturn's Equatorial jet's complex structure. *Nat. Commun.* **7**, 13262, DOI: 10.1038/ncomms13262 (2016).
7. Hueso, R. *et al.* Saturn atmospheric dynamics one year after Cassini: Long-lived features and time variations in the drift of the Hexagon. *Icarus* **336**, 113429, DOI: 10.1016/j.icarus.2019.113429 (2020). 1909.13849.
8. Simon, A. A., Hueso, R., Sánchez-Lavega, A. & Wong, M. H. Midsummer Atmospheric Changes in Saturn's Northern Hemisphere from the Hubble OPAL Program. *Planet. Sci. J.* **2**, 47, DOI: 10.3847/PSJ/abe40f (2021).
9. Lindzen, R. S. & Holton, J. R. A Theory of the Quasi-Biennial Oscillation. *J. Atmospheric Sci.* **25**, 1095–1107, DOI: 10.1175/1520-0469(1968)025<1095:ATOTQB>2.0.CO;2 (1968).
10. Andrews, D. G., Mahlman, J. D. & Sinclair, R. W. Eliassen-Palm Diagnostics of Wave-Mean Flow Interaction in the GFDL "SKYHI" General Circulation Model. *J. Atmospheric Sci.* **40**, 2768–2784, DOI: 10.1175/1520-0469(1983)040<2768:ETWATM>2.0.CO;2 (1983).
11. Baldwin, M. P. *et al.* The quasi-biennial oscillation. *Rev. Geophys.* **39**, 179–229, DOI: 10.1029/1999RG000073 (2001).
12. Leovy, C. B., Friedson, A. J. & Orton, G. S. The quasiquadrennial oscillation of Jupiter's equatorial stratosphere. *Nature* **354**, 380–382, DOI: 10.1038/354380a0 (1991).
13. Orton, G. S. *et al.* Thermal maps of Jupiter - Spatial organization and time dependence of stratospheric temperatures, 1980 to 1990. *Science* **252**, 537–542, DOI: 10.1126/science.252.5005.537 (1991).
14. Orton, G. S. *et al.* Spatial Organization and Time Dependence of Jupiter's Tropospheric Temperatures, 1980-1993. *Science* **265**, 625–631, DOI: 10.1126/science.265.5172.625 (1994).
15. Antuñano, A. *et al.* Fluctuations in Jupiter's equatorial stratospheric oscillation. *Nat. Astron.* **5**, 71–77, DOI: 10.1038/s41550-020-1165-5 (2021).

16. Reed, R. J., Campbell, W. J., Rasmussen, L. A. & Rogers, D. G. Evidence of downward propagating annual wind reversal in the equatorial stratosphere. *Journal of Geophysical Research* **66**, 813–818, DOI: 10.1029/JZ066i003p00813 (1961).

17. Burrage, M. D. *et al.* Long-term variability in the equatorial middle atmosphere zonal wind. *J. Geophys. Res. Atmosphere* **101**, 12,847–12,854, DOI: 10.1029/96JD00575 (1996).

18. Garcia, R. R., Dunkerton, T. J., Lieberman, R. S. & Vincent, R. A. Climatology of the semiannual oscillation of the tropical middle atmosphere. *J. Geophys. Res.* **102**, 26,019–26,032, DOI: 10.1029/97JD00207 (1997).

19. Showman, A. P., Tan, X. & Zhang, X. Atmospheric Circulation of Brown Dwarfs and Jupiter and Saturn-like Planets: Zonal Jets, Long-term Variability, and QBO-type Oscillations. *The Astrophys. J.* **883**, 4, DOI: 10.3847/1538-4357/ab384a (2019). 1807.08433.

20. Fletcher, L. N. *et al.* Disruption of Saturn's quasi-periodic equatorial oscillation by the great northern storm. *Nat. Astron.* **1**, 765–770, DOI: 10.1038/s41550-017-0271-5 (2017). 1803.07875.

21. Li, L. *et al.* Strong jet and a new thermal wave in Saturn's equatorial stratosphere. *Geophys. Res. Lett.* **35**, L23208, DOI: 10.1029/2008GL035515 (2008).

22. Fletcher, L. N., Irwin, P. G. J., Achterberg, R. K., Orton, G. S. & Flasar, F. M. Seasonal variability of Saturn's tropospheric temperatures, winds and para-H_2 from Cassini far-IR spectroscopy. *Icarus* **264**, 137–159, DOI: 10.1016/j.icarus.2015.09.009 (2016). 1509.02281.

23. Guerlet, S., Fouchet, T., Bézard, B., Simon-Miller, A. A. & Michael Flasar, F. Vertical and meridional distribution of ethane, acetylene and propane in Saturn's stratosphere from CIRS/Cassini limb observations. *Icarus* **203**, 214–232, DOI: 10.1016/j.icarus.2009.04.002 (2009).

24. Guerlet, S. *et al.* Meridional distribution of CH_3C_2H and C_4H_2 in Saturn's stratosphere from CIRS/Cassini limb and nadir observations. *Icarus* **209**, 682–695, DOI: 10.1016/j.icarus.2010.03.033 (2010).

25. Sinclair, J. A. *et al.* Seasonal variations of temperature, acetylene and ethane in Saturn's atmosphere from 2005 to 2010, as observed by Cassini-CIRS. *Icarus* **225**, 257–271, DOI: 10.1016/j.icarus.2013.03.011 (2013).

26. Fletcher, L. N. *et al.* Seasonal evolution of Saturn's polar temperatures and composition. *Icarus* **250**, 131–153, DOI: 10.1016/j.icarus.2014.11.022 (2015).

27. Sylvestre, M. *et al.* Seasonal changes in Saturn's stratosphere inferred from Cassini/CIRS limb observations. *Icarus* **258**, 224–238, DOI: 10.1016/j.icarus.2015.05.025 (2015).

28. Sinclair, J. A. *et al.* From Voyager-IRIS to Cassini-CIRS: Interannual variability in Saturn's stratosphere? *Icarus* **233**, 281–292, DOI: 10.1016/j.icarus.2014.02.009 (2014).

29. Friedson, A. J. & Moses, J. I. General circulation and transport in Saturn's upper troposphere and stratosphere. *Icarus* **218**, 861–875, DOI: 10.1016/j.icarus.2012.02.004 (2012).

30. Bardet, D. *et al.* Global climate modeling of Saturn's atmosphere. Part IV: Stratospheric equatorial oscillation. *Icarus* **354**, 114042, DOI: 10.1016/j.icarus.2020.114042 (2021).

31. Spiga, A. *et al.* Global climate modeling of Saturn's atmosphere. Part II: Multi-annual high-resolution dynamical simulations. *Icarus* **335**, 113377, DOI: 10.1016/j.icarus.2019.07.011 (2020).

32. Wheeler, M. & Kiladis, G. N. Convectively Coupled Equatorial Waves: Analysis of Clouds and Temperature in the Wavenumber-Frequency Domain. *J. Atmospheric Sci.* **56**, 374–399, DOI: 10.1175/1520-0469(1999)056<0374:CCEWAO>2.0.CO;2 (1999).

33. Haynes, P. H., McIntyre, M. E., Shepherd, T. G., Marks, C. J. & Shine, K. P. On the 'Downward Control' of Extratropical Diabatic Circulations by Eddy-Induced Mean Zonal Forces. *J. Atmospheric Sci.* **48**, 651–680, DOI: 10.1175/1520-0469(1991)048<0651:OTCOED>2.0.CO;2 (1991).

34. Plumb, R. A. Stratospheric transport. *J. Meteorol. Soc. Jpn.* **80**, 793–809, DOI: 10.2151/jmsj.80.793 (2002).

35. Seviour, W. J. M., Butchart, N. & Hardiman, S. C. The Brewer-Dobson circulation inferred from ERA-Interim. *Q. J. Royal Meteorol. Soc.* **138**, 878–888, DOI: 10.1002/qj.966 (2012).

36. Butchart, N. The Brewer-Dobson circulation. *Rev. Geophys.* **52**, 157–184, DOI: 10.1002/2013RG000448 (2014).

37. Kinnersley, J. S. & Pawson, S. The Descent Rates of the Shear Zones of the Equatorial QBO. *J. Atmospheric Sci.* **53**, 1937–1949, DOI: 10.1175/1520-0469(1996)053<1937:TDROTS>2.0.CO;2 (1996).

38. Dunkerton, T. On the Role of the Kelvin Wave in the Westerly Phase of the Semiannual Zonal Wind Oscillation. *J. Atmospheric Sci.* **36**, 32–41, DOI: 10.1175/1520-0469(1979)036\T1\textless{}0032:OTROTK\T1\textgreater{}2.0.CO;2 (1979).

39. Dunkerton, T. J. Nonlinear Propagation of Zonal Winds in an Atmosphere with Newtonian Cooling and Equatorial Wavedriving. *J. Atmospheric Sci.* **48**, 236–263, DOI: 10.1175/1520-0469(1991)048<0236:NPOZWI>2.0.CO;2 (1991).

40. Dunkerton, T. J. The role of gravity waves in the quasi-biennial oscillation. *J. Geophys. Res.* **102**, 26053–26076, DOI: 10.1029/96JD02999 (1997).

41. Friedson, A. J. New Observations and Modelling of a QBO-Like Oscillation in Jupiter's Stratosphere. *Icarus* **137**, 34–55, DOI: 10.1006/icar.1998.6038 (1999).

42. Li, X. & Read, P. L. A mechanistic model of the quasi-quadrennial oscillation in Jupiter's stratosphere. *Planet. Space Sci.* (2000).

43. Cosentino, R. G. *et al.* New Observations and Modeling of Jupiter's Quasi-Quadrennial Oscillation. *J. Geophys. Res. (Planets)* **122**, 2719–2744, DOI: 10.1002/2017JE005342 (2017).

44. Fletcher, L. N. *et al.* Thermal Structure and Dynamics of Saturn's Northern Springtime Disturbance. *Science* **332**, 1413, DOI: 10.1126/science.1204774 (2011).

45. Sánchez-Lavega, A. *et al.* Deep winds beneath Saturn's upper clouds from a seasonal long-lived planetary-scale storm. *Nature* **475**, 71–74, DOI: 10.1038/nature10203 (2011).

46. Sánchez-Lavega, A. *et al.* The great saturn storm of 2010–2011. In Baines, K. H., Flasar, F. M., Krupp, N. & Stallard, T. (eds.) *Saturn in the 21st Century*, Cambridge Planetary Science, 377–416, DOI: 10.1017/9781316227220.013 (Cambridge University Press, 2018).

47. Cavalié, T. *et al.* First direct measurement of auroral and equatorial jets in the stratosphere of Jupiter. *Astron. & Astrophys.* **647**, L8, DOI: 10.1051/0004-6361/202140330 (2021).

48. Benmahi, B. *et al.* Mapping the zonal winds of Jupiter's stratospheric equatorial oscillation. *Astron. & Astrophys.* **652**, A125, DOI: 10.1051/0004-6361/202141523 (2021).

49. Dubos, T. *et al.* DYNAMICO-1.0, an icosahedral hydrostatic dynamical core designed for consistency and versatility. *Geosci. Model. Dev.* **8**, 3131–3150, DOI: 10.5194/gmd-8-3131-2015 (2015).

50. Meurdesoif, Y. XIOS presentation given at the Workshop on Scalable IO in climate models, Hamburg, Germany, available on `http://forge.ipsl.jussieu.fr/ioserver/raw-attachment/wiki/WikiStart/XIOS_IO_Workshop_Hamburg.pdf` (2012).

51. Meurdesoif, Y. XIOS presentation given at the Second Workshop on Coupling Technologies for Earth System Models (CW2013, NCAR), Boulder, Colorado-USA, available on `http://forge.ipsl.jussieu.fr/ioserver/raw-attachment/wiki/WikiStart/XIOS-BOULDER.pdf` (2013).

52. Guerlet, S. *et al.* Global climate modeling of Saturn's atmosphere. Part I: Evaluation of the radiative transfer model. *Icarus* **238**, 110–124, DOI: 10.1016/j.icarus.2014.05.010 (2014).

53. Wordsworth, R. D. *et al.* Is Gliese 581d habitable? Some constraints from radiative-convective climate modeling. *Astron. & Astrophys.* **522**, A22, DOI: 10.1051/0004-6361/201015053 (2010). 1005.5098.

54. Charnay, B. *et al.* Exploring the faint young Sun problem and the possible climates of the Archean Earth with a 3-D GCM. *J. Geophys. Res. (Atmospheres)* **118**, 10,414–10,431, DOI: 10.1002/jgrd.50808 (2013).

55. Leconte, J. *et al.* 3D climate modeling of close-in land planets: Circulation patterns, climate moist bistability, and habitability. *Astron. & Astrophys.* **554**, A69, DOI: 10.1051/0004-6361/201321042 (2013). 1303.7079.

56. Rothman, L. S. *et al.* The HITRAN2012 molecular spectroscopic database. *J. Quant. Spectrosc. Radiat. Transf.* **130**, 4–50, DOI: 10.1016/j.jqsrt.2013.07.002 (2013).

57. Wordsworth, R. Transient conditions for biogenesis on low-mass exoplanets with escaping hydrogen atmospheres. *Icarus* **219**, 267–273, DOI: 10.1016/j.icarus.2012.02.035 (2012). 1106.1411.

58. Mellor, G. L. & Yamada, T. Development of a Turbulence Closure Model for Geophysical Fluid Problems (Paper 2R0808). *Rev. Geophys. Space Phys.* **20**, 851, DOI: 10.1029/RG020i004p00851 (1982).

59. Hourdin, F., Le van, P., Forget, F. & Talagrand, O. Meteorological Variability and the Annual Surface Pressure Cycle on Mars. *J. Atmospheric Sci.* **50**, 3625–3640, DOI: 10.1175/1520-0469(1993)050<3625:MVATAS>2.0.CO;2 (1993).

60. Cabanes, S., Spiga, A. & Young, R. M. B. Global Climate Modelling of Saturn's atmosphere. Part III: Global statistical picture of zonostrophic turbulence in high-resolution 3D-turbulent simulations. *Icarus* **345**, 113705, DOI: 10.1016/j.icarus.2020.113705 (2020).

61. Kiladis, G. N., Wheeler, M. C., Haertel, P. T., Straub, K. H. & Roundy, P. E. Convectively coupled equatorial waves. *Rev. Geophys.* **47**, RG2003, DOI: 10.1029/2008RG000266 (2009).

62. Maury, P. & Lott, F. On the presence of equatorial waves in the lower stratosphere of a general circulation model. *Atmospheric Chem. & Phys.* **14**, 1869–1880, DOI: 10.5194/acp-14-1869-2014 (2014).

63. Andrews, D. G., Holton, J. R. & Leovy, C. B. *Middle Atmosphere Dynamics* (Academic Press, 1987).

64. Vallis, G. K. *Atmospheric and Oceanic Fluid Dynamics* (2006).

A Extended data figures

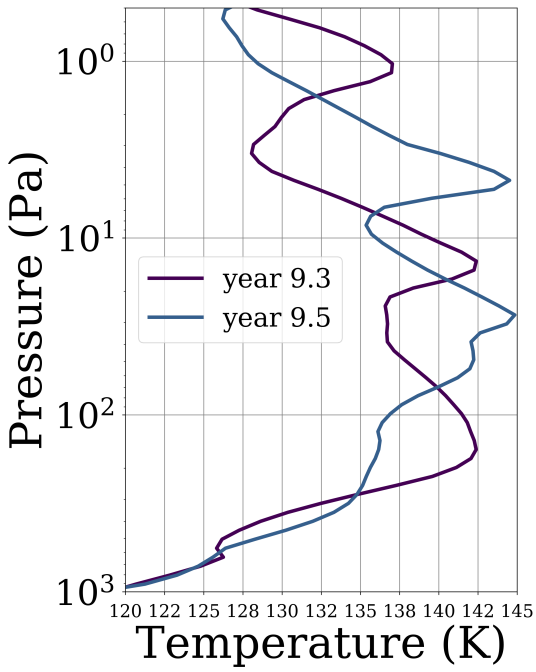

Figure A.1. Temperature phase of modelled Saturn's equatorial oscillation. Zonal-mean temperature profiles for two different times to highlight temperature oscillation phases change. These profiles are averaged between $\pm 2^\circ$ of latitude.

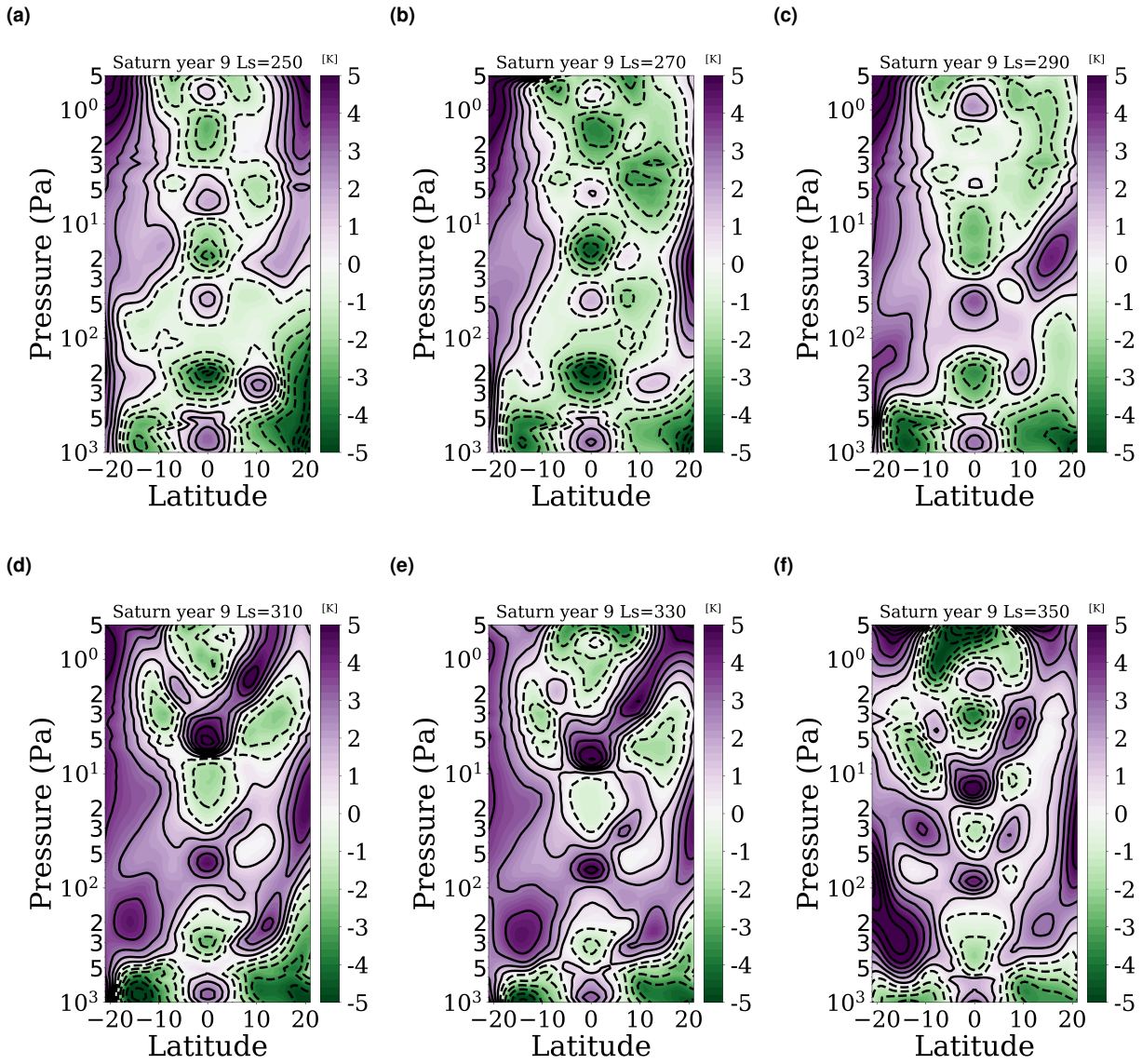

Figure A.2. Descent over time of equatorial temperature anomalies. Altitude/latitude sections of zonal-mean temperature departures from mean temperature, which varies with seasons in Saturn's stratosphere at six dates for the ninth simulated Saturn year. To see the variations of the descent of the temperature anomalies over 10 Saturn years, we refer the reader to the video in additional data available here: https://doi.org/10.14768/6494348c-3304-4838-a379-a7ccfefac872

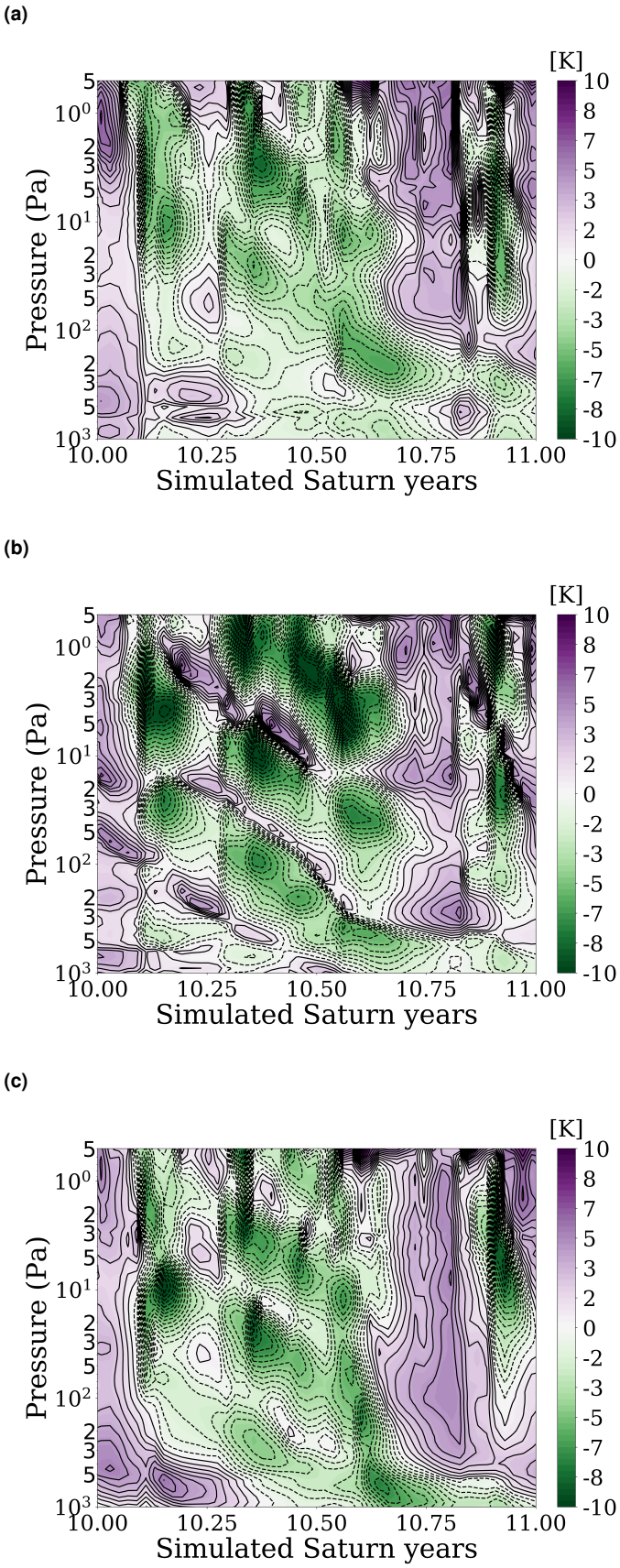

Figure A.3. Vertical structure of temperature anomalies at and surrounding the equator. Altitude-time cross section of the zonal-mean temperature anomalies at (A.3a) 11°N, at (A.3b) the equator and at (A.3c) 11°S for the tenth simulated Saturn years.

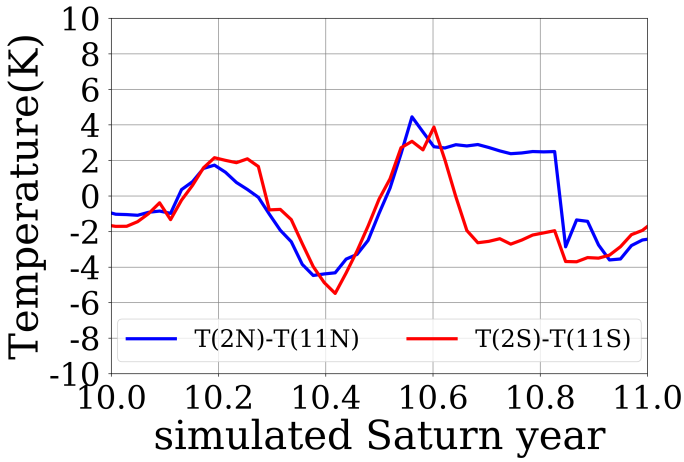

Figure A.4. Differences of zonal-mean temperature at two different planetocentric latitudes over time to highlight the equatorial oscillation periodicity. These figures were produced so as to be comparable to ground-based observations and can be compared to ref.[2]: the temperature was averaged between 100 and 200 Pa to account for the coarse vertical resolution of nadir observations, and were also averaged from 0 to $\pm 3°$ and from ± 10 and $\pm 12°$ of latitude to emulate the 3° spatial resolution of these observations. Then, we compute temperature differences between the average 0-3°N and the average 10-12°N (denoted by blue line) and between the average 0-3°S and the average 10-12°S (denoted by red line).

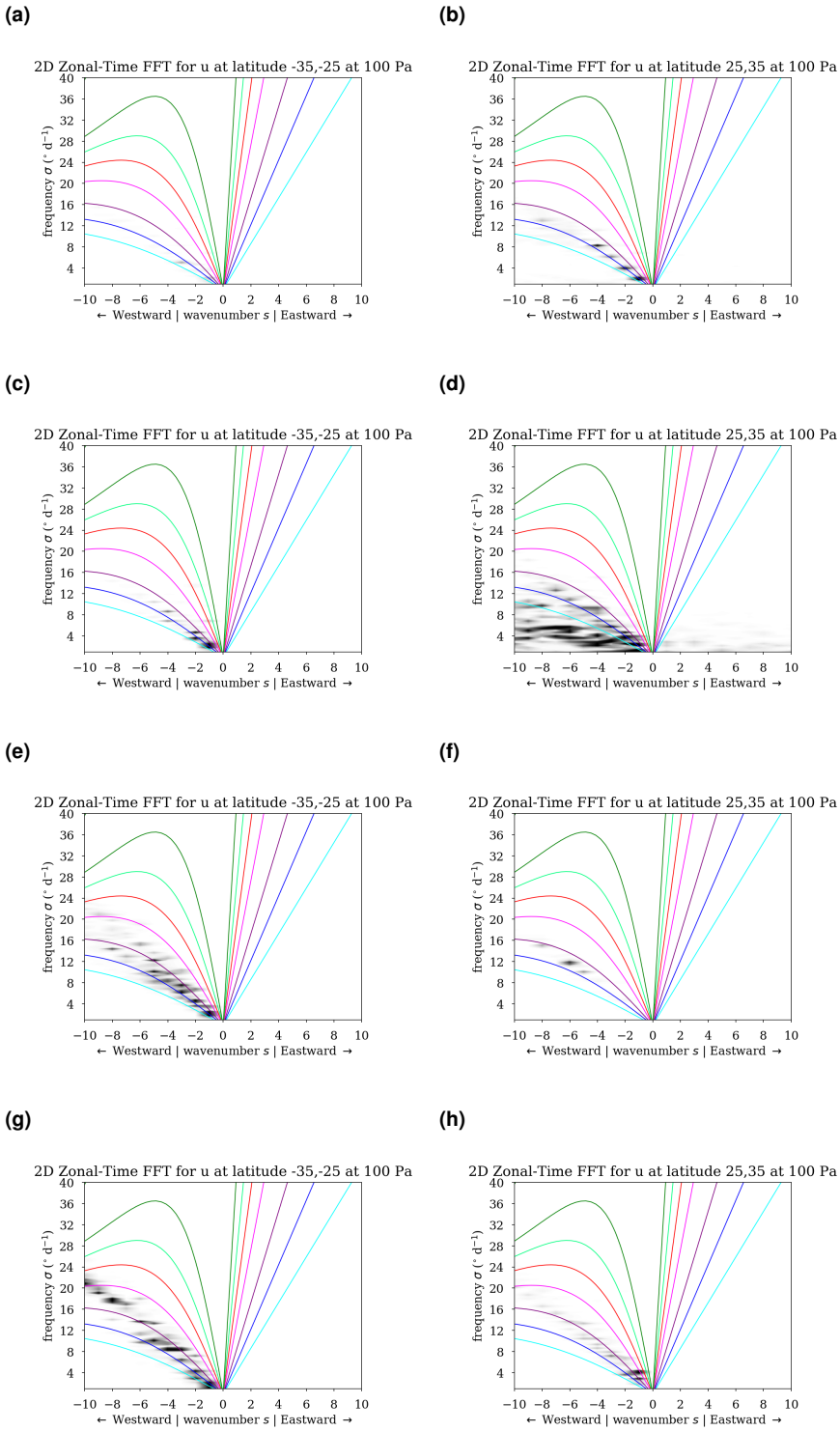

Figure A.5. Seasonal activity of planetary-scale waves around ±30° of latitude to highlight Rossby waves surf zones driving the main downward branch of the seasonal inter-hemispheric circulation. Two-dimensional Fourier transforms[32] of the symmetric component of u – A.5a and A.5b northern winter from Ls=250° to Ls=340°, A.5c and A.5d northern spring from Ls=340° to Ls=70°, A.5e and A.5f northern summer from Ls=70° to Ls=160° and A.5g and A.5h northern autumn from Ls=160° to Ls=250° – at 100 Pa. Gray shaded areas depict the waves identified by the spectral analysis. Color curves represent relation dispersion from the linear theory. Seven equivalent depths are used for theoretical curves: 5 km (cyan), 10 km (blue), 20 km (purple), 50 km (magenta), 100 km (red), 200 km (light green), 500 km (dark green).

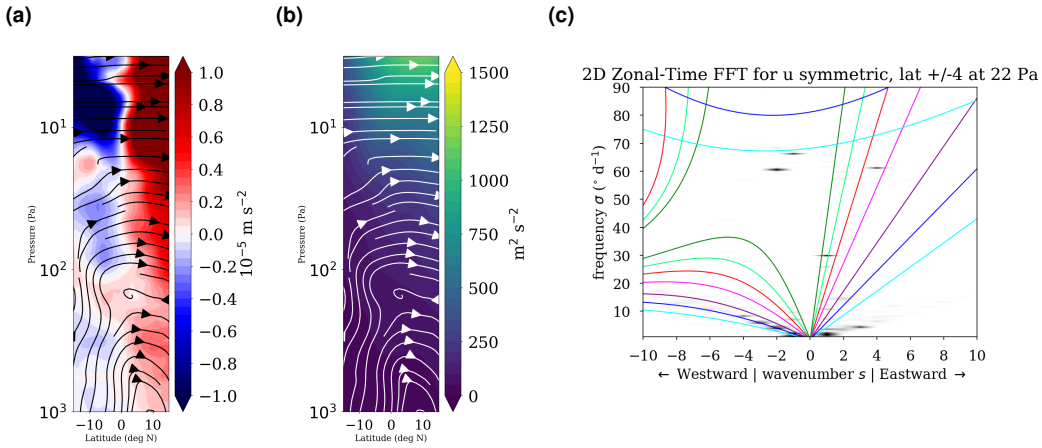

Figure A.6. Equatorial eddy- and RMC-forcing during the northern winter season. Northern winter seasonal mean (Ls=250° to Ls=340°) of RMC (A.6a) and of the eddy-kinetic energy (A.6b), defined by EKE = $\frac{1}{2}\left(u'^2 + v'^2\right)$, superimposed to the residual mean circulation ($\overline{v^*}$, $\overline{\omega^*}$ in streamlines) for a typical simulated year from DYNAMICO-Saturn. The associated spectra is shown in A.6c to identify waves involved in the interplay between Saturn's equatorial oscillation and Saturn's inter-hemispheric circulation.

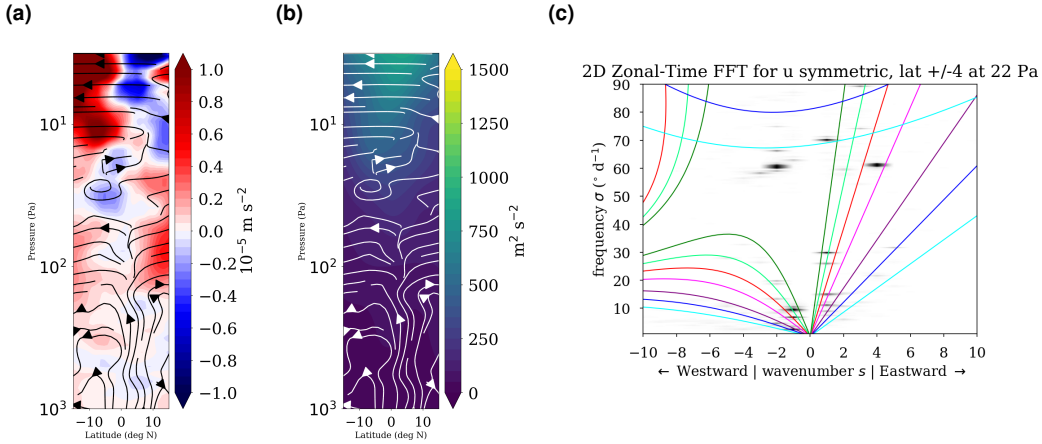

Figure A.7. Equatorial eddy- and RMC-forcing during the northern spring season. Same as Figure A.6 for northern spring seasonal mean (Ls=340° to Ls=70°).

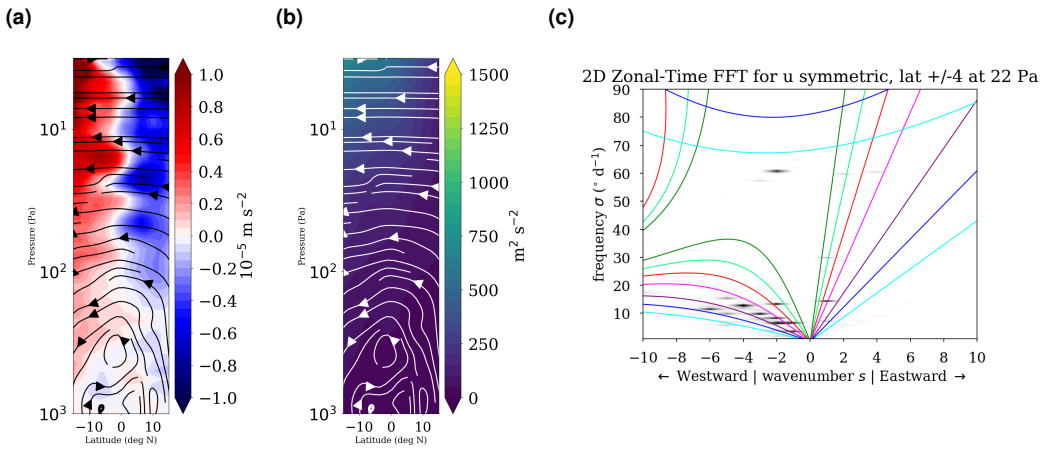

Figure A.8. Equatorial eddy- and RMC-forcing during the northern summer season. Same as Figure A.6 for northern summer seasonal mean (Ls=70° to Ls=160°).

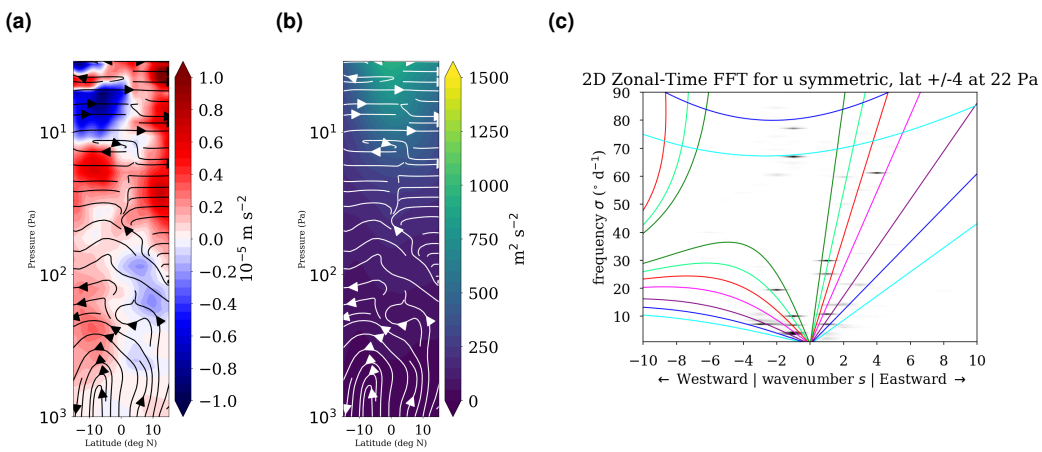

Figure A.9. Equatorial eddy- and RMC-forcing during the northern autumn season. Same as Figure A.6 for northern autumn seasonal mean (Ls=190° to Ls=280°). The seasonal mean for the autumn equinox is shift by 30° of Ls to clearly brought out the fall overturn, that occurs later is the season compared to the spring overturn.